Dual-Band Dual-Polarized Wearable Button Array with Miniaturized Radiator

Jiahao Zhang, *Student Member, IEEE*, Sen Yan, *Member, IEEE*, Xiaomu Hu, and Guy A. E. Vandenbosch, *Fellow, IEEE*

***Abstract*—A dual-band dual-polarized wearable array is proposed, based on a miniaturized innovating button radiator topology. The diameter of the rigid button is only 19.5 mm (0.29 λ at 4.5 GHz), which optimizes the users' comfort, and makes it the smallest up to date in literature. The operational bands are 4.50-4.61 GHz and 5.04-5.50 GHz. The antenna thus covers the 4.5-4.6 unlicensed future 5th generation (5G) communication band for the internet of things (IoT), and the 5.1-5.5 GHz wireless local area network (WLAN) band, respectively. Two orthogonal linear polarizations are obtained in each band. A low mutual coupling between the button antenna elements (below -18 dB) and between the two ports within each element (below -20 dB) is achieved, guaranteeing a good diversity performance. The envelope correlation coefficient (ECC) and the specific absorption rate (SAR) performance are also analyzed. In order to demonstrate the robustness of the button antenna and to mimic realistic situations, a more complicated asymmetrical ground plane model of the button antenna is studied for the first time. A prototype of a two-element button array has been fabricated. The measurement results match well with the simulations. A 10-element button array is studied within the context of a 3-D channel model, taking into account the button element's radiation pattern. A high achievable spectral efficiency (SE) is obtained.**

***Index Terms*—Wearable antennas, antenna arrays, button antennas, miniaturization.**

I. Introduction

DURING the last decade, wireless body area networks (WBAN) are developing rapidly in the field of physical training, navigation, health monitoring, and so on [1]-[3]. As an essential part of WBAN, a wearable antenna realizes the wireless data transmission from an on-body sensor node to an off-body station, or to another on-body senor node. Several categories of wearable antennas have been studied in the past, such as conductive textile antennas [4], [5], flexible and semi-flexible substrate based antennas [6], [7], liquid metal antennas [8], [9], button antennas [10], [11], conformal antennas [12], [13], and miniaturized integrated antennas [14], [15], etc. Among these, button antennas show some clear advantages, since they can be easily mounted on clothes at several locations around the human body. Moreover, the button antenna is normally rigid in most circumstances, which usually guarantees a better radiation performance than a pure textile wearable antenna [16].

Multiple-input-multiple-output (MIMO) can be implemented to increase the data rates, overcome multipath phenomena, and reduce power consumption [17]. Recently, studies have been made to implement MIMO in WBAN [4], [18]. Wearable MIMO technologies hold great promise for their rich potential in future WBAN systems [19]. In most cases, the planar antenna topology is chosen [4], [18]. Although a series of buttons instead of a single one is a common feature in most clothes, so that considering a wearable button array is actually a quite natural consideration, as far as the authors can see, wearable button arrays have not been realized before.

Modern wireless communication systems usually have to combine multiple standards with different working frequencies and protocols. This means that antennas with multiple bands and functions are required. Dual-polarized antennas with orthogonal polarizations are also in high demand in WBAN systems, since they have the potential to overcome the polarization loss by human body movements. Moreover, polarization diversity can be introduced to address the issue of multipath fading and improve the channel capacity. Multiband wearable button antennas have been studied in [20], [21]. However, polarization diversity is not achieved there. A dual-band button antenna with two different modes in each band is proposed in [22]. However, the button size is quite large, which may affect the comfort of the users, and pattern diversity is not realized. Effort has also been done to study a circularly polarized button antenna to overcome the polarization loss [10]. However, the proposed antenna has only one band, which limits its applications. Moreover, pattern diversity is not achieved.

It is a quite innovating and logical idea to design a button antenna starting from the following requirements, dedicated to WBAN applications: (1) multi-band to meet various communication standards, (2) dual-polarized pattern diversity to improve the data rates and overcome the polarization mismatch, and (3) miniaturized button size to optimize the users' comfort (meaning a smaller rigid PCB size). As far as the authors can see, these three properties have not been

Manuscript received July 2, 2019. This work was partly supported by the Research Foundation – Flanders (F.W.O.) Postdoctoral Fellowship (No. 12O1217N). (Corresponding author: Sen Yan.)

J. Zhang, X. Hu and G. A. E. Vandenbosch are with the ESAT-TELEMIC Research Division, Department of Electrical Engineering, KU Leuven, 3001 Leuven, Belgium (e-mail: jiahao.zhang@esat.kuleuven.be). S. Yan is with the Faculty of Electronics and Information, Xi'an Jiaotong University, Xi'an, Shanxi 710049, China (e-mail: sen.yan@xjtu.edu.cn).

Color versions of one or more of the figures in this paper are available online at http://ieeexplore.ieee.org.

Digital Object Identifier

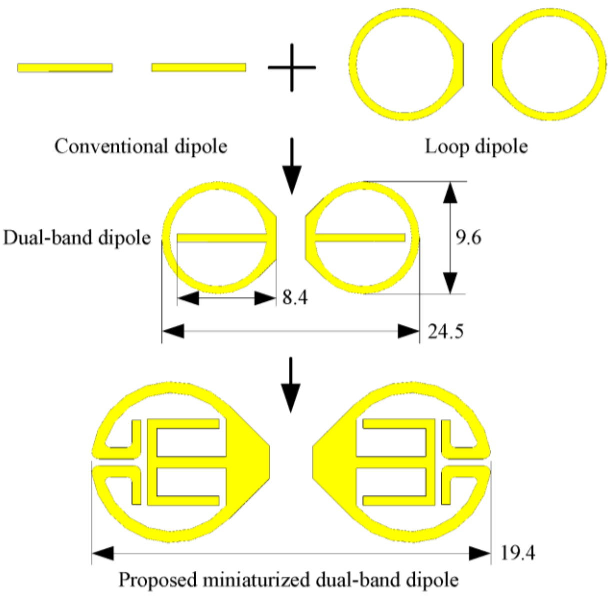

Fig. 1 Design process of the proposed miniaturized dual-band dipole. The yellow indicates copper. The substrate and ground are hidden for simplicity. Dimensions are in mm.

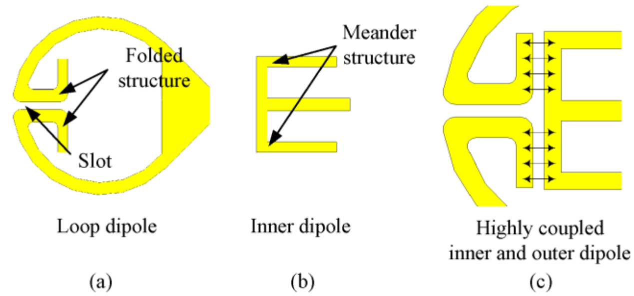

Fig. 2 (a) Loaded outer loop dipole. (b) Loaded inner dipole. (c) Highly coupled inner and outer dipole.

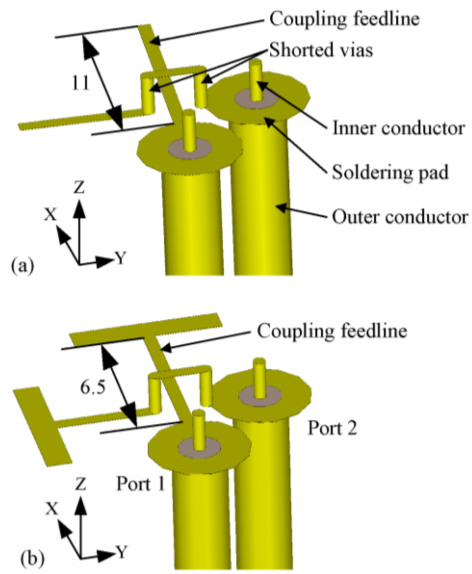

Fig. 3 (a) Conventional feeding topology with straight coupling feedline. (b) Proposed feedline with T-shaped structure loading. Dimensions are in mm.

simultaneously reached for a wearable button antenna.

In this paper, a dual-band dual-polarized button antenna is proposed. A small-size rigid PCB is used as a basis for the button element. A flexible conducting textile (clothes) acts as the antenna ground, and a semi-rigid coaxial cable is used to feed the proposed antenna. Such topology guarantees a robust antenna structure while maintaining the users' comfort. A realistic button-up situation with consideration of a complicated asymmetrical ground plane model is studied. A wearable button array is then realized for the first time. A low inter-element mutual coupling (the mutual coupling between the two elements) and inner-element mutual coupling (the mutual coupling between the two ports of a single element) are achieved, which guarantees a good diversity performance. This array is analyzed within the context of a 3D channel model.

The organization of the paper is as follows. In section II, the working mechanism and detailed design of the button antenna are given. In section III, the simulations and on-body measurement results are introduced. The button array is then analyzed prior to a discussion on the array performance, all in section IV. Finally, this work is summarized together with concluding remarks in section V.

II. Button Antenna Design

The frequency domain solver in the commercial software CST Microwave Studio [23] was used for all designs. The targeted two bands are the 4.5 GHz and 5.2 GHz bands. Two orthogonal radiation patterns (horizontal and vertical) are chosen for pattern diversity, and for compensation of polarization mismatch. A broadside radiation pattern rather than an omni-directional radiation pattern is used, since a higher channel capacity is normally achieved with broadside pattern MIMO elements, according to [18], and our previous study [24]. Taking all these facts into consideration, the grounded crossed dipole topology is selected in this design. The design process of the button antenna starts from a grounded dipole antenna which is fed by coaxial cables. The antenna ground is formed by textile materials, which are easily integrated with clothes. A broadside radiation pattern is thus achieved by adding the ground. The highly coupled inner meander dipole and outer loop dipole are proposed to excite the higher and lower resonance respectively, and are located on a rigid PCB board (button PCB). In order to miniaturize the size of the button, a compact dual-band dipole is used. The design process is shown in Fig. 1. A conventional wire dipole (inner dipole) and a conventional loop dipole (outer dipole) are first combined to achieve the dual-band operation. To obtain the targeted frequency bands, the length of the conventional dual-band dipole should be 24.5 mm, according to simulations (the same antenna topology as in the proposed design except the radiator). Additional structures are then loaded to miniaturize the size. A slot, which is connected to a folded copper structure, is introduced at the end of the outer loop dipole, see Fig. 2 (a). A meander structure is loaded to increase the length of current flow of the inner dipole, see Fig. 2 (b). Note that the folded copper structure of the outer dipole is placed close to the inner meander structure. The induced currents again increase the electrical length of both the inner

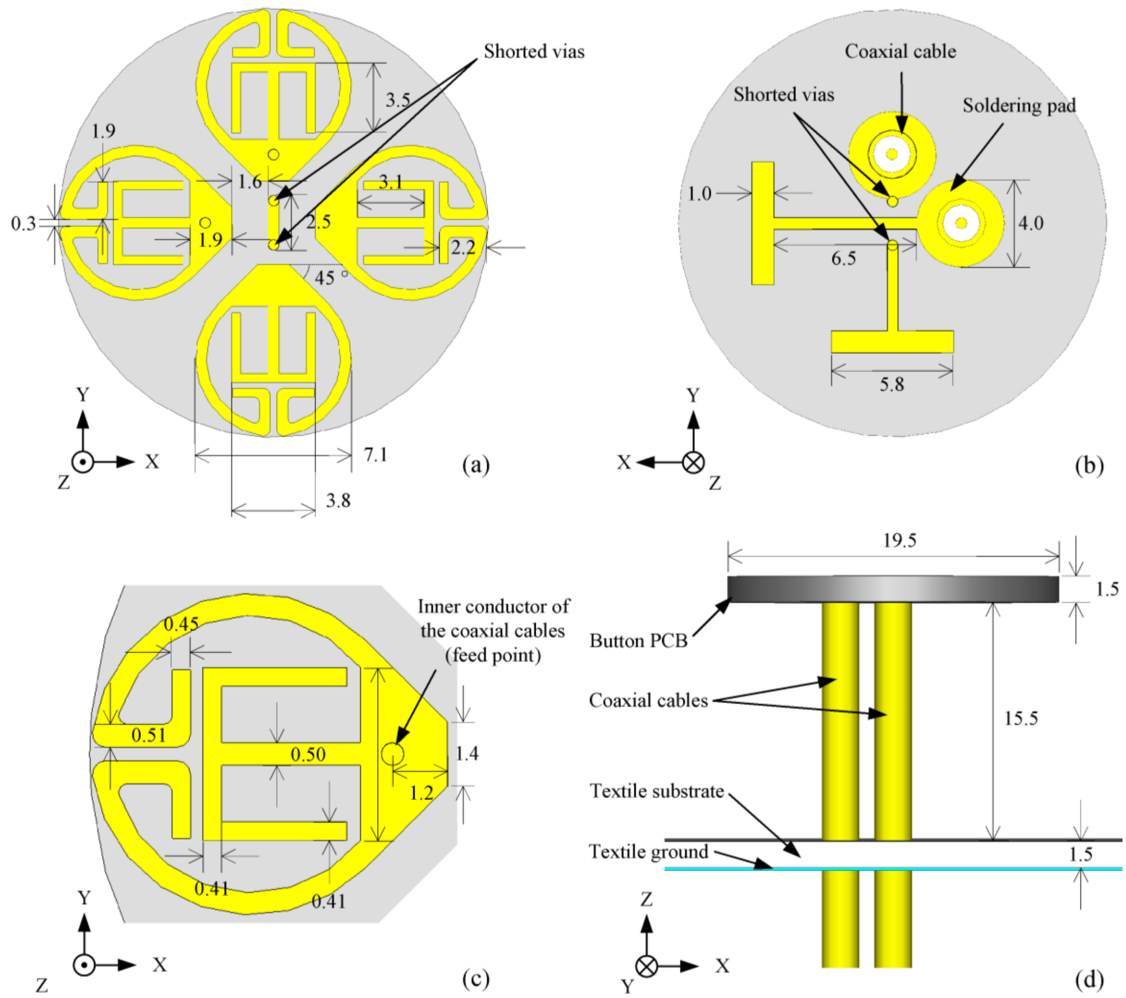

Fig. 4 Topology of the button antenna: (a) top view of the rigid substrate, (b) bottom view of the rigid substrate, (c) zoom of the radiator structure, (d) side view of the button antenna. Dimensions are in mm.

and outer dipoles, see Fig. 2 (c). Dual-band operation is thus achieved by these two compact sized and highly coupled radiator structures. A perpendicularly placed dual-band dipole is the added to obtain the orthogonal polarization. The area of the button PCB is reduced by 37 % compared with the conventional design.

The button antenna is fed by coaxial cables. The inner conductor of the coaxial cable is directly soldered to one side of the dual-band dipole, which is on the top side of the PCB broad. And the outer conductor is soldered to a soldering pad on the back side of the PCB broad. The soldering pad is then connected to a coupling feedline, see Fig. 3, which couples the energy to the other side of the dipole antenna. A conventional straight coupling feedline is shown in Fig. 3 (a). In order to reach a similar performance (operating bands) as the proposed button antenna, the length of the straight feedline should be 11 mm, according to simulations. In order to achieve a small-size button, a shorter feedline is desired. A conventional feedline can be modeled as an open-ended transmission line. Shortening the length of the feedline decreases the inductance. The T-shaped structure is therefore loaded at the end of the feedline. It is equivalent to two parallel open stubs, which increases the inductance again [1]. Note that the feeding topologies of the two ports are slightly different, since the feedline of port 2 is turned to avoid an intersection. This was achieved by using the shorted vias and the conducting strip on top layer of the rigid button shown in Fig. 3 and Fig. 4. Fig. 3 (b) gives a perspective view of the feeding networks of the two orthogonal dipoles.

In order to optimize the user's comfort, normally a rigid button has a dimensional restriction. In our design, the main purpose is to minimize the size of the rigid substrate which carries the radiator structure, since the antenna ground is flexible. The miniaturization is achieved by both the highly coupled radiation structure, and the T-shaped coupling feeding network.

The geometry of the proposed antenna is shown in Fig. 4. The particle swarm optimization algorithm in CST was used when fine tuning the dimensions. The radiator structures of the proposed antenna are constructed on the top side of a button shaped rigid 1.524 mm thick RO4003C substrate, with relative permittivity 3.55 and dielectric loss tangent 0.0027 [25], respectively. The feeding structures are located on the back side (a small part on the top side) of the substrate. The button substrate is located on top of a textile substrate (non-conductive 1.5 mm thick felt textile, with relative permittivity 1.4 and dielectric loss tangent 0.044 [26]). The antenna ground is

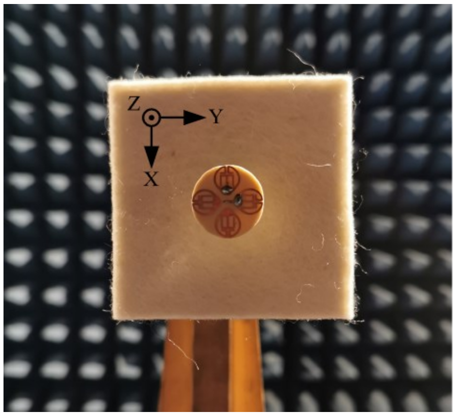

Fig. 5 Prototype of the button antenna.

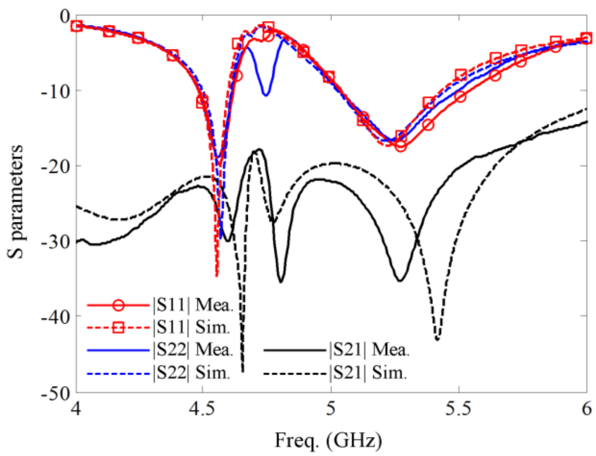

Fig. 6 S parameters of the button antenna. The red lines = |S11|, the blue lines = |S22|, the black lines = |S21|. The solid lines indicate the measurement results, the dashed lines indicate the simulation results.

TABLE I

REALIZED GAIN AND TOTAL EFFICIENCY

	Freq. (GHz)	Gain (dBi)		Efficiency (%)	
		Mea.	Sim.	Mea.	Sim.
Port 1	4.55	7.4	7.8	86	88
	5.2	7.6	7.6	93	94
Port 2	4.55	7.5	7.7	85	88
	5.2	7.4	7.5	92	94

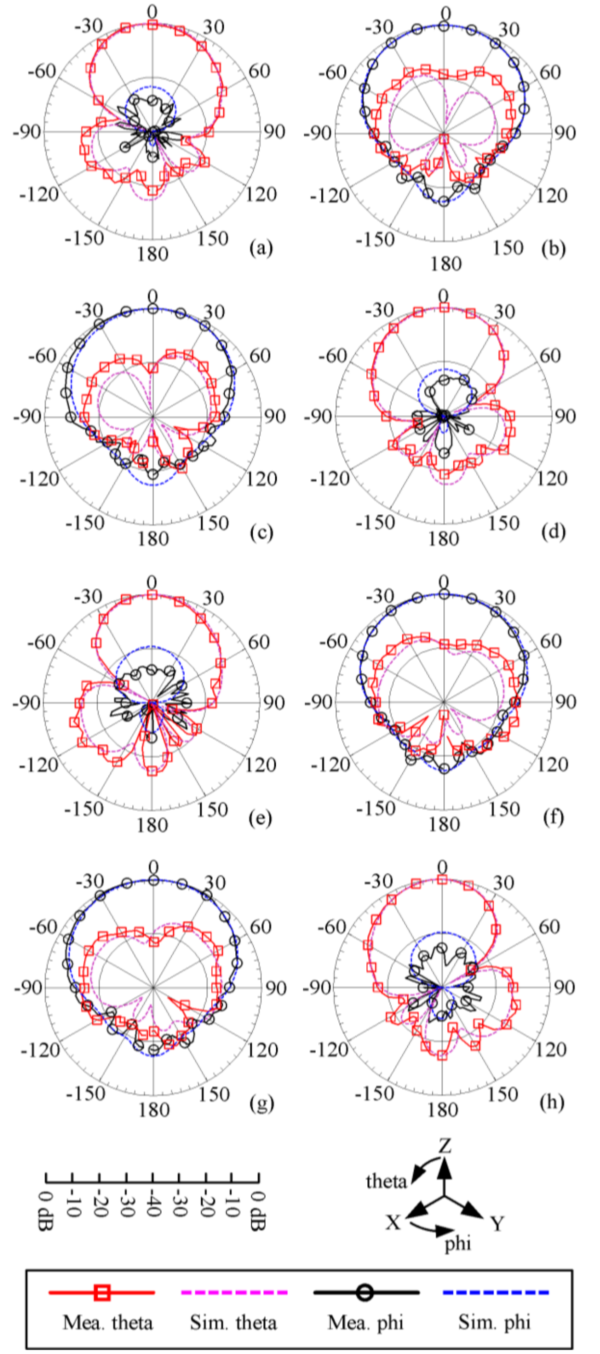

Fig. 7 Radiation patterns: Port 1 at 4.55 GHz, (a) XZ plane, (b) YZ plane. Port 2 at 4.55 GHz, (c) XZ plane, (d) YZ plane. Port 1 at 5.2 GHz, (e) XZ plane, (f) YZ plane. Port 2 at 5.2 GHz, (g) XZ plane, (h) YZ plane.

formed using a 0.17 mm thick ShieldIt superconductive textile with an estimated conductivity of 118000 S/m [27], which is located on the bottom side of the textile substrate. Two semi-rigid coaxial cables [28] are connected to the button substrate to feed the antenna, and also act as supporters. This way of working avoids additional supporters, which makes the proposed button antenna more realistic. The outer conductors of the cables are also soldered to the textile antenna ground. Note that the semi rigid cables not only act as feeding structures, but also act as supporters to connect the button to the textile structure (clothes in realistic situations). We would like to emphasize that the proposed topology is robust enough for wearable applications because of the following reasons. (1) The two semi-rigid cables are simultaneously used as supporters, which increases the robustness. (2) The cables are soldered to the button PCB, which means that the relative positioning of the cables and the button will not change. (3) The button-up situation is analyzed in section III, part B. In this case, a textile layer is inserted between the button PCB and the textile ground, via the button PCB, like in normal clothes. The button-up action was repeated for more than 100 times, and the robustness was not affected at all.

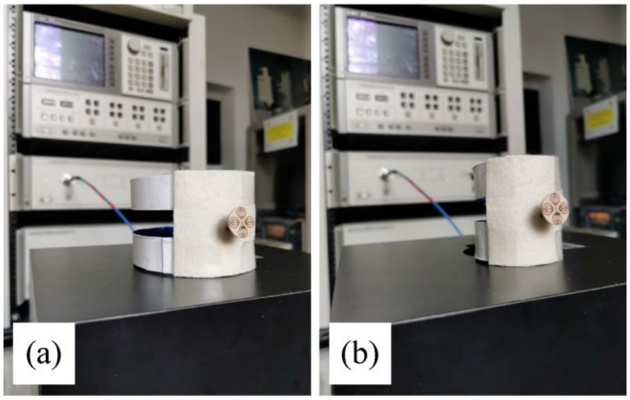

Fig. 8 Antenna under bending: (a) bending radius=50 mm, (b) bending radius=30 mm.

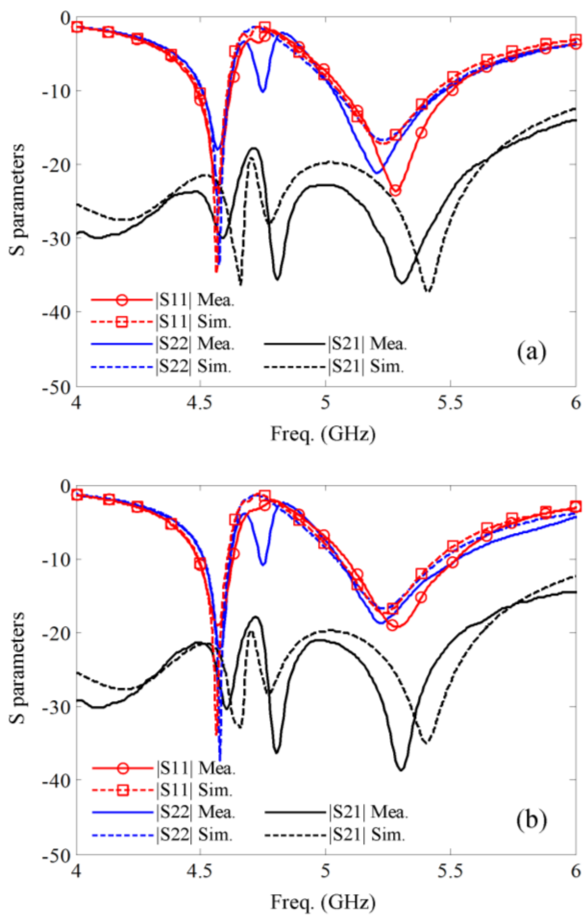

Fig. 9 S parameters when bent along X-axis. (a) Radius=50 mm. (b) Radius=30 mm. The red lines = |S11|, the blue lines = |S22|, the black lines = |S21|. The solid lines indicate the measurement results, the dashed lines indicate the simulation results.

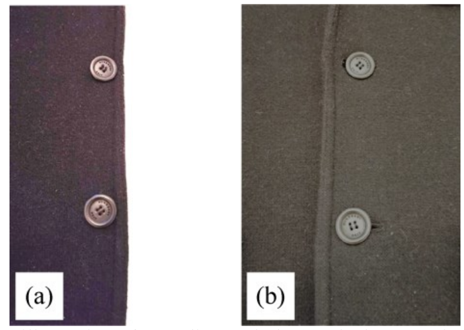

Fig. 10 An illustration of an ordinary cloth. (a) The buttons always locate near the edge of the cloth. (b) Button-up situation.

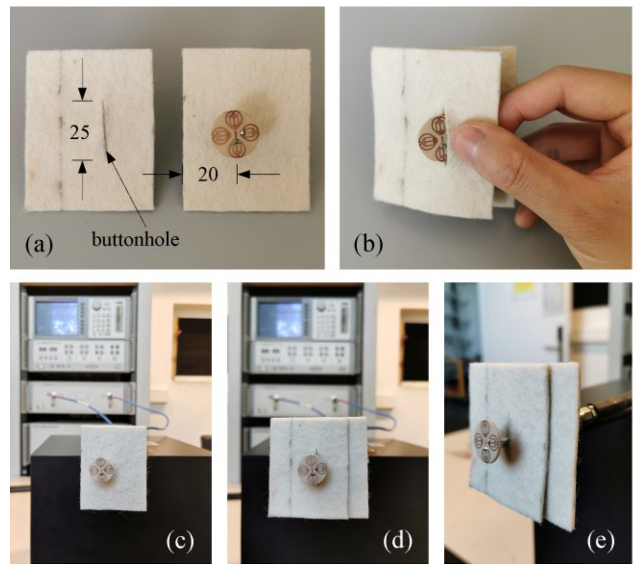

Fig. 11 Antenna prototype with asymmetrical ground. (a) Button locates 20 mm away from the edge. (b) Button-up action. Measurement setup: (c) button with asymmetrical ground, (d) button with additional textile layer, (e) perspective view.

III. Simulation and Measurement Results

A. Antenna Performance in Free Space

A prototype was fabricated to validate the proposed concept, see Fig. 5. The S-parameters were measured with an HP 8510 Vector Network Analyzer, and are compared with the simulation results in Fig. 6. The measured results match well with the simulated results. Two resonances are clearly seen for both ports. The measured overlapping bands for both port 1 and port 2 are 4.50-4.61 GHz and 5.04-5.50 GHz, respectively, which covers the 4.5-4.6 unlicensed future 5G communication band for the internet of things (IoT), and the 5.1-5.5 GHz WLAN band [29], [30].

The radiation patterns were measured in the anechoic chamber at KU Leuven. Fig. 7 gives the normalized radiation patterns of both ports. A good agreement between the measurements and simulations is achieved. The patch-like broadside radiation patterns are clearly observed for both bands. The front-to-back ratio (FBR) is always higher than 15 dB, which means that a good forward radiation performance is obtained. The cross-polarization level of all radiation patterns is below -10 dB. The realized gain and total efficiency of the proposed button antenna are summarized in Table I.

B. Antenna Performance on Body

A bending analysis is implemented in this part in order to mimic realistic situations. The reflection coefficient of the proposed antenna is investigated when bent over a cylinder along the X-axis. Cylinders with radii of 50 and 30 mm were used, see Fig. 8. The S-parameter results are presented in Fig. 9.

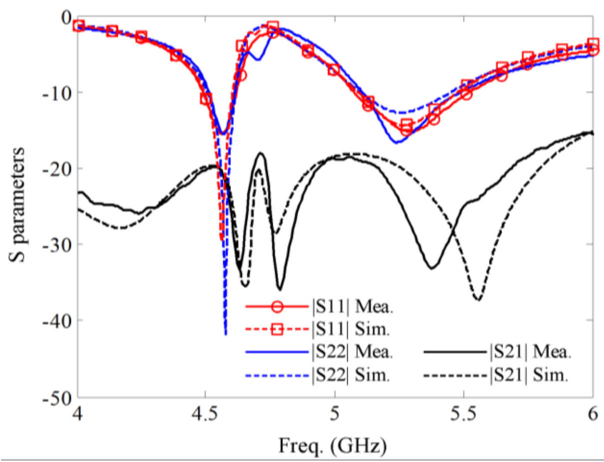

Fig. 12 S parameters of the asymmetrical case. The red lines = |S11|, the blue lines = |S22|, the black lines = |S21|. The solid lines indicate the measurement results, the dashed lines indicate the simulation results.

Fig. 13 Measured antenna located on a human body.

Both the higher and lower resonances do not change much under bending, since the radiator is located on a rigid PCB which doesn't change during bending.

Most button antenna designs consider the button in the middle of a ground [10], [11], [21], [22]. However, in realistic situations, the button normally locates near the edge of the clothes, which means that the flexible ground may be asymmetrical. What is more, when the cloth is buttoned-up, another layer of textile material may insert between the rigid button and the textile ground, which may affect the performance of the button antenna. An illustration of an ordinary cloth is given in Fig. 10. As far as the authors can see, these issues were not considered in previous research in literature. An asymmetrical ground is developed to simulate the button-up situation. Consider the button located 20 mm away from the edge of the clothes, see Fig. 11 (a). The textile substrate and ground are asymmetrical in this case, which obviously affects the radiation patterns. In order to compensate the change of the radiation pattern, an additional piece of ground is introduced. Note that there is a slot (button hole) in the additional textile layer, see Fig. 11 (a), just like in normal clothes. The additional textile layer is inserted between the button and the original textile layer via the button hole. When the cloth is buttoned-up, the two pieces of ground form the antenna ground together, see Fig. 11 (d) and (e). In this case, the S-parameters of the button antenna are not significantly affected, see Fig. 12. Note also that the button-up action does not break or bend the semi-rigid cables (supporters). The stable antenna performances and the firm structures (button and cables) verify the robustness of the proposed topology under realistic wearing situations.

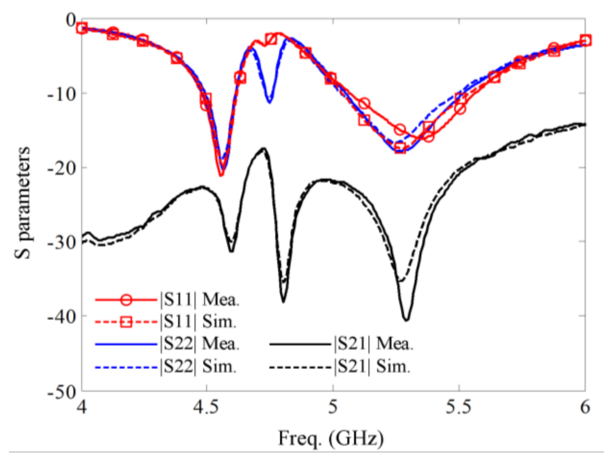

Fig. 14 Measured S parameters on body. The red lines = |S11|, the blue lines = |S22|, the black lines = |S21|. The solid lines indicate the results on body, the dashed lines indicate the results in free space.

The button antenna was tested on a volunteer's body. It was located on the chest of the volunteer, see Fig. 13. The measured S-parameter results are compared with the results in free space and given in Fig 14. As we can see from Fig. 14, the antenna constantly covers the needed band when worn on body.

In order to ensure the conformance to safety regulations, the specific absorption rate (SAR) was evaluated and averaged over 10 g of biological tissue, based on the IEEE/IEC 62704-1 standard. Two simplified models for human tissue (on the chest and the arm) were built in CST MWS. The chest model defines 20 mm of space behind the antenna to mimic a practical antenna to skin distance due to clothing. It consists of a skin layer, a fat layer, and a muscle layer, with thicknesses 3 mm, 7 mm, and 60 mm, respectively [1]. The arm model defines 10 mm of space behind the antenna. It consists of a skin layer, a fat layer, and a muscle layer, with thicknesses 2 mm, 5 mm, and 20 mm, and an inner bone layer with radius 13 mm, respectively [31]. The antenna is bent with a radius of 60 mm, when worn on the arm. The root mean square input power for each port is set at 0.5 W. The SAR distribution is plotted in Fig. 15. Note that only the SAR result of port 1 is given, since port 1 and port 2 are quite similar. The results show that the SAR result is below 0.0554 W/kg at 4.55 GHz, and below 0.0711 W/kg at 5.2 GHz, respectively, when the antenna is located on the chest, and below 0.0664 W/kg at 4.55 GHz, and below 0.0942 W/kg at 5.2 GHz, respectively, when the antenna is located on the arm. These values are much lower than the European standard threshold of 2 W/kg, thanks to the shielding by the conductive textile ground. Note also that the on-body antenna performance (on the chest and on the arm), more specifically the S-parameters and the total efficiencies, is almost the same as in the case of free space. However, the realized gain is higher than in free space when the antenna is located on the chest, and lower than in free space when the antenna is located on the arm. The reason is simple. The chest acts as a reflector, which increases the forward radiation (Z>0 °). When the antenna is located on the arm, the antenna ground plane is bent, see Fig. 15

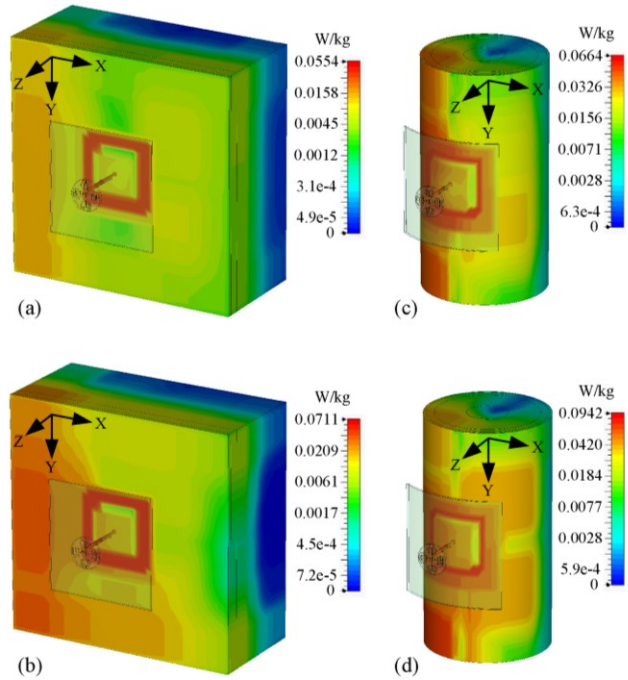

Fig. 15 SAR distribution when the antenna is located on the chest: at (a) 4.55 GHz, and (b) 5.2 GHz, and on the arm: at (c) 4.55 GHz, and (d) 5.2 GHz.

TABLE II
COMPARISON OF DUAL-BAND OR WIDEBAND CROSSED DIPOLE ANTENNAS

Ref.	Lowest Freq. (GHz)	Radiator size		Diameter (λ)
		in mm	in λ	
[32]	1.7	54*54	0.306*0.306	0.433
[33]	1.7	57.4*57.4	0.325*0.325	0.460
[34]	1.66	55.7*55.7	0.308*0.308	0.436
[35]	1.69	51*51	0.287*0.287	0.406
[36]	1.7	50*50	0.283*0.283	0.400
[37]	1.7	45*45	0.255*0.255	0.361
This work	4.5	π*9.75^2	π*0.146^2	0.292

(c) and (d). This means that the effective size of the reflector is reduced, which decreases the forward radiation. The on-body radiation patterns are compared with the ones in free space in Fig. 16. The effect of the body is very small. When the distance between the antenna and the human body is changed, for example, the distance between the chest and antenna (Fig. 15 (a) and (b)) is changed to 10 mm, the antenna performance will not change much, e. g. the difference in bandwidth (both higher and lower band) between the two cases is less than 0.01 GHz.

A robust performance of the proposed button antenna is achieved. What is more, to the best knowledge of the authors, the smallest radiator size is achieved for a dual-band and dual-polarized dipole topology, see the comparison in Table II. Since a button is always round shaped, the size (diameter) of the substrate which carries the radiator is determined by looking at the round area that is covered by the radiator and the feeding network. Despite a miniaturized radiator size and a

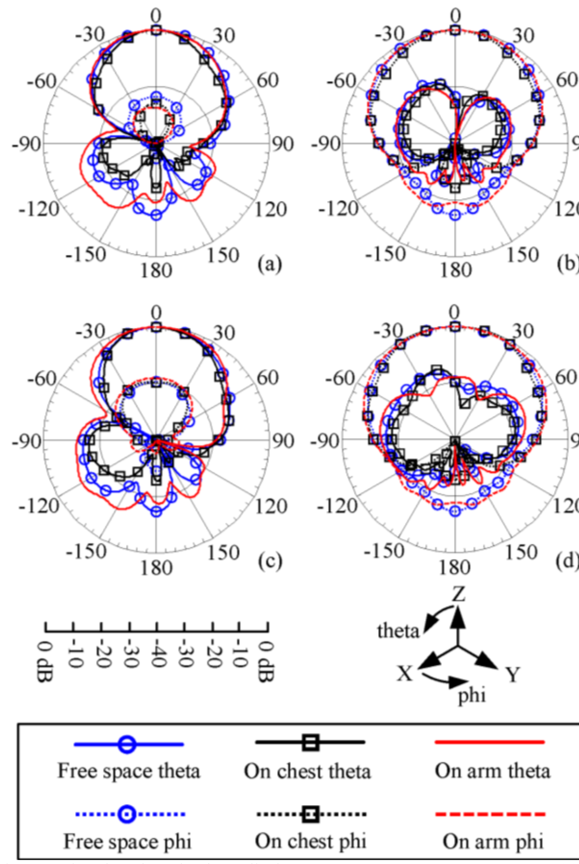

Fig. 16 Simulated on-body radiation patterns: Port 1 at 4.55 GHz, (a) XZ plane, (b) YZ plane, at 5.2 GHz, (c) XZ plane, (d) YZ plane.

simple topology, the antenna retains a good performance for wearable applications.

IV. BUTTON ANTENNA ARRAY

A. Prototype of Two-Element Array

A prototype of the button array was fabricated with two antenna elements, see Fig. 17. The distance between the two buttons is 40 mm (0.60 λ at 4.5 GHz, 0.69 λ at 5.2 GHz), and the ground size is 110*70 mm. The S parameters of the two-element array are given in Fig. 18. As we can see from Fig. 18, the reflection coefficients (S11, S22, S33, S44) of the two elements almost do not change. The mutual coupling (S21, S31, S41, S32, S42, S43) between the two elements is quite low. The maximum value occurs between port 2 and port 4 (S42): -19 dB around 4.55 GHz, and -18 dB around 5.2 GHz, since these two ports are co-polarized. The measured peak mutual coupling results (S42 at 4.55 GHz and 5.2 GHz) are slightly lower (1.5 dB lower) than the simulated results. The reason is that the two elements are not perfectly aligned.

In order to investigate the MIMO performance of the button array, the envelope correlation coefficient (ECC) is studied based on the two-element array. As a simple and useful way to approximately evaluate the diversity performance of the proposed antenna, the ECC is calculated from the S-parameters [38].

$$\rho \approx \frac{|S11^{*}S12 + S21^{*}S22|^2}{|(1-|S11|^2-|S21|^2)(1-|S22|^2-|S12|^2)|} \quad (1)$$

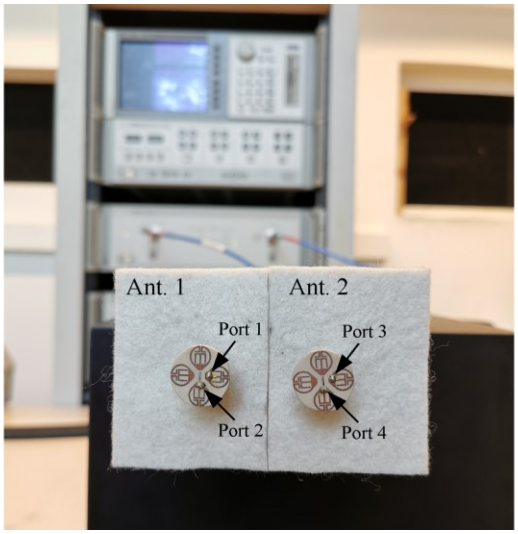

Fig. 17 Prototype of the two-element button antenna array.

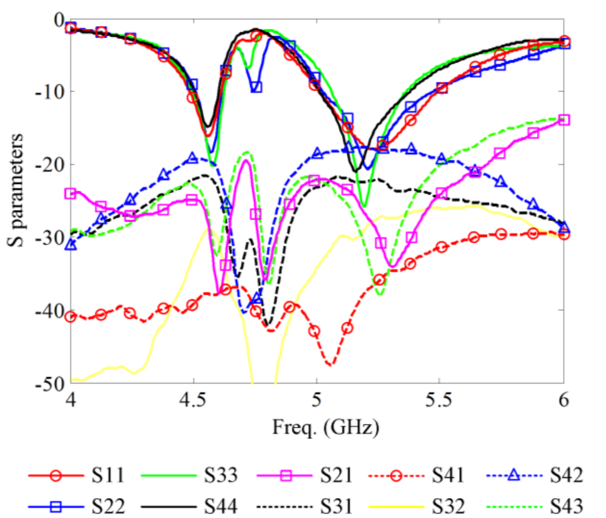

Fig. 18 Measured S parameters of the two-element button antenna array.

This ECC is shown in Fig. 19. The values are less than 0.035 for all cases, which is very acceptable for MIMO systems.

B. Spectral Efficiency of the Proposed Button Array

In many previous studies, the antenna radiation pattern is assumed to be omni-directional when describing the channel model. In this paper, the 3-D spatial evaluation is performed by including the radiation patterns as functions of azimuth θ and elevation φ. A WBAN MIMO system that contains an *M*-element base station and an *N*-element mobile user terminal (in this case, the wearable button array) is studied. Each element of the user terminal has *K* different radiation patterns. The MIMO channel is described by the matrix $\mathbf{H} = [\boldsymbol{h}_1\boldsymbol{h}_2, \ldots, \boldsymbol{h}_N]$, which represents the channel between the base station and the user terminal [39]:

$$\boldsymbol{h}_n = \boldsymbol{G}(\theta,\varphi)\boldsymbol{a}(\theta,\varphi)\boldsymbol{v_n} \quad (2)$$

$\boldsymbol{G}(\theta,\varphi)$ represents the radiation pattern of the user terminal antenna array.

$$\boldsymbol{G}(\theta,\varphi) = diag\{(\boldsymbol{G}_1(\theta,\varphi))^{1/2}, \ldots, \boldsymbol{G}_n((\theta,\varphi))^{1/2}\} \quad (3)$$

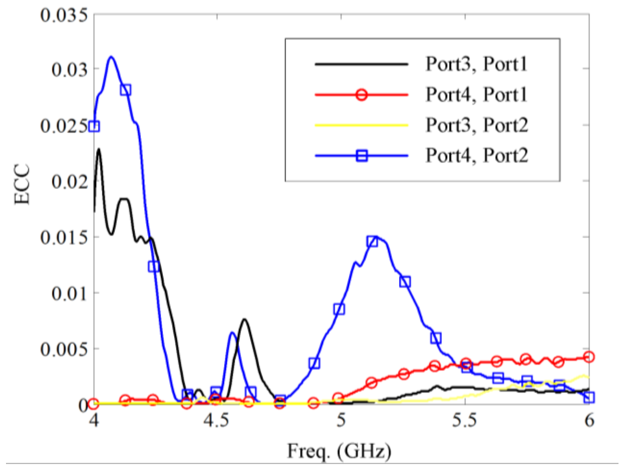

Fig. 19 ECC results calculated from the measured S parameters.

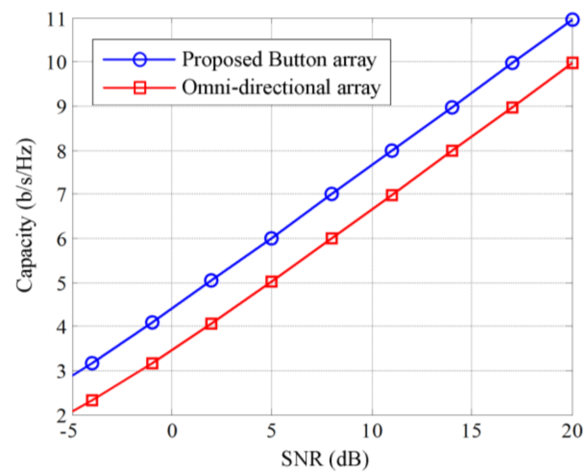

Fig. 20 SE performance of the 10-element button antenna array.

where $\boldsymbol{G}_n(\theta,\varphi) = [G_{n,1}(\theta,\varphi), \ldots, G_{n,k}(\theta,\varphi)]^{\mathrm{T}}$ indicates that each antenna element has *K* different radiation patterns [40]. $\boldsymbol{a}(\theta,\varphi)$ is the steering vector with different angles of arrival (AoA) for the *n*th user terminal antenna, which can be obtained in [24]. $\boldsymbol{v_n}$ represents a standard complex Gaussian vector.

We consider a single line-of-sight (LoS) scenario with *M*=8 and *N*=10 (*K*=2 when the proposed dual-polarized button elements are used). A linear array topology is assumed for the button array. The radiation pattern of the transmit antenna at the base station is assumed to be omni-directional. The element spacing of the button array is 0.6 λ, where λ is the wavelength at 4.5 GHz. We fix the AoA $\varphi = 90$ °, and assume the AoA $|\theta| < 90$ °. The channel is considered ergodic.

The SE of this system is calculated and compared to the configuration with *M*=8, *N*=10, *K*=1 (the radiation pattern of the user terminal antenna element is omni-directional). By using the measured radiation patterns at the lower resonance of the proposed button antenna element, the down-link achievable SE is computed and shown in Fig. 20. As we expect, the achievable SE of the proposed array is 20% higher than the one of the contrasted omni-directional array.

V. Conclusion

In this paper, a dual-band dual-polarized wearable button antenna array is proposed based on the crossed dipole topology. The main novelty and contribution are the following. (1) A wearable button array is realized, (2) achieving a dual-band dual-polarized topology with the smallest radiator size in literature. (3) Even when considering realistic button-up actions, a considerable performance is always obtained. This last aspect has never been studied before. The diameter of the realized rigid button is only 19.5 mm (0.29 λ). The profile of the proposed antenna is 18 mm (0.27 λ). By designing an artificial magnetic conductor (AMC) [41], [42] to replace the ground plane, in future work the profile can be further reduced. The button antenna prototype covers the 4.50-4.61 GHz band and the 5.04-5.50 GHz bands simultaneously, and thus has a potential for 5G, IoT, and WLAN applications. The button antenna element is analyzed both in free space and on body. The button antenna array is analyzed based on a 3-D channel model. The simple topology and robust performance enable large scale industrial production.

References

[1] J. Zhang, S. Yan, and G. A. E. Vandenbosch, "A miniature feeding network for aperture-coupled wearable antennas," *IEEE Transactions on Antennas and Propagation,* vol. 65, no. 5, pp. 2650-2654, May 2017.

[2] J. Mao, H. Yang, and B. Zhao, "An investigation on ground electrodes of capacitive coupling human body communication," *IEEE Transactions on Biomedical Circuits and Systems*, vol. 11, no. 4, pp. 910-919, Aug. 2017.

[3] G. R. Tsouri, S. R. Zambito, and J. Venkataraman, "On the benefits of creeping wave antennas in reducing interference between neighboring wireless body area networks," *IEEE Transactions on Biomedical Circuits and Systems*, vol. 11, no.1, pp. 153-160, Feb. 2017.

[4] S. Yan, P. J. Soh, and G. A. E. Vandenbosch, "Dual-band textile MIMO antenna based on substrate-integrated waveguide (SIW) technology," *IEEE Transactions on Antennas and Propagation,* vol. 63, no. 11, pp. 4640-4647, Nov. 2015.

[5] D. Patron, W. Mongan, T. P. Kurzweg, A. Fontecchio, G. Dion, E. K. Anday, and K. R. Dandekar, "On the use of knitted antennas and inductively coupled RFID tags for wearable applications," *IEEE Transactions on Biomedical Circuits and Systems*, vol. 10, no. 6, pp. 1047-1057, Dec. 2016.

[6] A. S. Alqadami, K. S. Bialkowski, A. T. Mobashsher, and A. M. Abbosh, "Wearable electromagnetic head imaging system using flexible wideband antenna array based on polymer technology for brain stroke diagnosis," *IEEE Transactions on Biomedical Circuits and Systems*, vol. 13, no. 1, pp. 124-134, Feb. 2019.

[7] J. Zhang, S. Yan, X. Hu, and G. A. E. Vandenbosch, "Mutual coupling suppression for on-body multi-antenna systems," *IEEE Transactions on Electromagnetic Compatibility*, accepted.

[8] M. Cosker, L. Lizzi, F. Ferrero, R. Staraj, and J. M. Ribero, "Realization of 3-D flexible antennas using liquid metal and additive printing technologies," *IEEE Antennas and Wireless Propagation Letters*, vol. *16*, pp. 971-974, 2017.

[9] G. J. Hayes, J. H. So, A. Qusba, M. D. Dickey, and G. Lazzi, "Flexible liquid metal alloy (EGaIn) microstrip patch antenna," *IEEE Transactions on Antennas and Propagation*, vol. 60, no. 5, pp. 2151-2156, May 2012.

[10] X. Hu, S. Yan, and G. A. E. Vandenbosch, "Compact circularly polarized wearable button antenna with broadside pattern for U-NII worldwide band applications," *IEEE Transactions on Antennas and Propagation*, vol. 67, no. 2, pp. 1341-1345, Feb. 2019.

[11] B. Sanz-Izquierdo, F. Huang, and J. C. Batchelor, "Covert dual-band wearable button antenna," *Electronics Letters*, vol. 42, no. 12, pp. 668-670, Jun. 2016.

[12] Y. Wang, J. Zhang, F. Peng, and S. Wu, "A glasses frame antenna for the applications in Internet of Things," *IEEE Internet of Things Journal*, early access.

[13] L. Yang, L. J. Martin, D. Staiculescu, C. P. Wong, and M. M. Tentzeris, "Conformal magnetic composite RFID for wearable RF and bio-monitoring applications," *IEEE Transactions on Microwave Theory and Techniques*, vol. 56, no. 12, pp. 3223-3230, Dec. 2008.

[14] C. H. Tseng, L. T. Yu, J. K. Huang, and C. L. Chang, "A wearable self-injection-locked sensor with active integrated antenna and differentiator-based envelope detector for vital-sign detection from chest wall and wrist," *IEEE Transactions on Microwave Theory and Techniques*, vol. 66, no. 5, pp. 2511-2521, May 2018.

[15] Z. H. Jiang, M. D. Gregory, and D. H. Werner, "Design and experimental investigation of a compact circularly polarized integrated filtering antenna for wearable biotelemetric devices," *IEEE Transactions on Biomedical Circuits and Systems*, vol. 10, no. 2, pp. 328-338, Apr. 2016.

[16] S. Yan, and G. A. E. Vandenbosch, "Design of wideband button antenna based on characteristic mode theory," *IEEE Transactions on Biomedical Circuits and Systems,* vol. 12, no. 6, pp. 1383-1391, Dec. 2018.

[17] D. Gesbert, M. Shafi, D. S. Shiu, P. J. Smith, and A. Naguib, "From theory to practice: An overview of MIMO space-time coded wireless systems," *IEEE Journal on Selected Areas in Communications*, vol. 21, no. 3, Apr. 2013.

[18] Y. Ouyang, D. J. Love, and W. J. Chappell, "Body-worn distributed MIMO system," *IEEE Transactions on Vehicular Technology,* vol. 58, no. 4, pp. 1752-1765, May 2009.

[19] J. Zhang, S. Yan, and G. A. E. Vandenbosch, "Realization of dual band pattern diversity with a CRLH-TL inspired reconfigurable metamaterial," *IEEE Transactions on Antennas and Propagation*, vol. 66, no. 10, pp. 5130-5138, Oct. 2018.

[20] B. Sanz-Izquierdo, F. Huang, J. C. Batchelor, "Covert dual-band wearable button antenna," *Electronics Letters*, vol. *42*, no. 12, pp. 668-670, Jun. 2006.

[21] X. Hu, S. Yan, and G. A. E. Vandenbosch, "Wearable button antenna for dual-band WLAN applications with combined on and off-body radiation patterns," *IEEE Transactions on Antennas and Propagation*, vol. *65*, no. 3, pp. 1384-1387, Mar. 2017.

[22] X. Y. Zhang, H. Wong, T. Mo, and Y. F. Cao, "Dual-band dual-mode button antenna for on-body and off-body communications," *IEEE Transactions on Biomedical Circuits and Systems*, vol. *11*, no. 4, pp. 933-941, Aug. 2017.

[23] Microwave Studio. (2016). *Computer Simulation Technology (CST)*. [Online]. Available: http://www.cst.com/Products/CSTMWS/

[24] C. M. Chen, V. Volski, L. Van der Perre, G. A. E. Vandenbosch, and S. Pollin, "Finite large antenna arrays for Massive MIMO: characterization and system impact," *IEEE Transactions on Antennas and Propagation*, vol. 65, no. 12, pp. 6712-6720, Dec. 2017.

[25] Rogers Corp. (2018). *Specification Sheet—RO4000 Series*. [Online]. Available: https://www.rogerscorp.com/documents/726/acs/RO4000-LaminatesData-Sheet.pdf

[26] RS Components Inc. (2013). *Specification Sheet—Felt Sheet*. [Online]. Available: http://uk.rs-online.com/web/p/felt-sheets/7336779

[27] LessEMF Inc. (2013). *Specification Sheet—ShieldIt Super*. [Online]. Available: http://www.lessemf.com/1220.pdf

[28] HUBER+SUHNER (2019). *Data Sheet—Cable*. [Online]. Available: http://www.inexim.pl/Download/Karty%20katalogowe%20RF/Kable/kable%20SEMI%20RIGID/EZ_86_TP_M17.pdf

[29] Nokia (2017). *5G deployment below 6 GHz*. [Online]. Available: https://www.rrt.lt/wp-content/uploads/2018/10/Nokia_5G_Deployment_below_6GHz_White_Paper_EN.pdf

[30] GSMA (2018). *5G Spectrum*. [Online]. Available: https://www.gsma.com/spectrum/wp-content/uploads/2018/11/5G-Spectrum-Positions.pdf

[31] Z. H. Jiang, D. E. Brocker, P. E. Sieber, and D. H. Werner, "A compact, low-profile metasurface-enabled antenna for wearable medical body-area network devices," *IEEE Transactions on Antennas and Propagation*, vol. 62, no. 8, pp. 4021-4030, Aug. 2014.

[32] D. Z. Zheng, and Q. X. Chu, "A miniaturized wideband dual-polarized antenna for base-station applications," in *International Symposium on Antennas and Propagation (ISAP)*, pp. 1-2, Oct. 2017.

[33] M. Li, Q. L. Li, B. Wang, C. F. Zhou, and S. W. Cheung, "A low-profile dual-polarized dipole antenna using wideband AMC reflector," *IEEE Transactions on Antennas and Propagation*, vol. 66, no. 5, pp. 2610-2615, May 2018.

[34] Y. Chen, W. Lin, S. Li, and A. Raza, "A broadband ±45° dual-polarized multidipole antenna fed by capacitive coupling," *IEEE Transactions on Antennas and Propagation*, vol. 66, no. 5, pp. 2644-2649, May 2018.

[35] L. H. Wen, S. Gao, C. X. Mao, Q. Luo, W. Hu, Y. Yin, and X. Yang, “A wideband dual-polarized antenna using shorted dipoles,” *IEEE Access*, vol. 6, pp. 39725-39733, 2018.

[36] C. F. Ding, X. Y. Zhang, Y. Zhang, Y. M. Pan, and Q. Xue, “Compact Broadband Dual-Polarized Filtering Dipole Antenna With High Selectivity for Base-Station Applications,” *IEEE Transactions on Antennas and Propagation*, vol. 66, no. 11, pp. 5747-5756, Nov. 2018.

[37] L. H. Wen, S. Gao, Q. Luo, C. X. Mao, W. Hu, Y. Yin, Y. Zhou, and Q. Wang “Compact Dual-Polarized Shared-Dipole Antennas for Base Station Applications,” *IEEE Transactions on Antennas and Propagation*, vol. 66, no. 12, pp. 6826-6834, Dec. 2018.

[38] Q. Rao, and D. Wang, “A compact dual-port diversity antenna for long-term evolution handheld devices,” *IEEE Transactions on Vehicular Technology*, vol. 59, no. 3, pp. 1319-1329, Mar. 2010.

[39] K. Zheng, S. Ou, and X. Yin, “Massive MIMO channel models: A survey,” *International Journal of Antennas and Propagation*, vol. 2014, Jun. 2014, Art. no. 848071.

[40] M. Sanchez-Fernandez, E. Rajo-Iglesias, O. Quevedo-Teruel, and M. L. Pablo-Gonzalez, “Spectral efficiency in MIMO systems using space and pattern diversities under compactness constraints,” *IEEE Transactions on Vehicular Technology*, vol. 57, no. 3, pp. 1637-1645, May 2009.

[41] G. Li, H. Zhai, L. Li, C. Liang, R. Yu, and S. Liu, “AMC-loaded wideband base station antenna for indoor access point in MIMO system,” *IEEE Transactions on Antennas and Propagation*, vol. 63, no. 2, pp. 525-533. Feb. 2015.

[42] W. Lin, S. L. Chen, R. W. Ziolkowski, and Y. J. Guo, “Reconfigurable, wideband, low-profile, circularly polarized antenna and array enabled by an artificial magnetic conductor ground,” *IEEE Transactions on Antennas and Propagation*, vol. 66, no. 3, pp. 1564-1569, Mar. 2018.